Supporting Information

[6,6]-Phenyl-C_{61}-Butyric Acid Methyl Ester/Cerium Oxide Bilayer Structure as Efficient and Stable Electron Transport Layer for Inverted Perovskite Solar Cells

Rui Fang,[†‡] Shaohang Wu,[†‡] Weitao Chen,[†‡] Zonghao Liu,[†‡] Shasha Zhang,[†] Rui Chen,[†] Youfeng Yue,[§] Linlong Deng,[⊤] Yi-Bing Cheng,[⊥] Liyuan Han,[#] Wei Chen[†]*

[†] Wuhan National Laboratory for Optoelectronics, Huazhong University of Science and Technology, Luoyu Road 1037, Wuhan, 430074, China

[§] Electronics and Photonics Research Institute, National Institute of Advanced Industrial Science and Technology (AIST), 1-1-1 Higashi, 305-8565, Tsukuba, Japan

[⊤] Pen-Tung Sah Institute of Micro-Nano Science and Technology, Xiamen University, Xiamen 361005, China.

[⊥] Department of Materials Science and Engineering, Monash University, Victoria 3800, Australia

[#] Research Network and Facility Services Division, National Institute for Materials Science, Japan

[*] Corresponding author E-mail: wnlochenwei@mail.hust.edu.cn (Wei Chen).

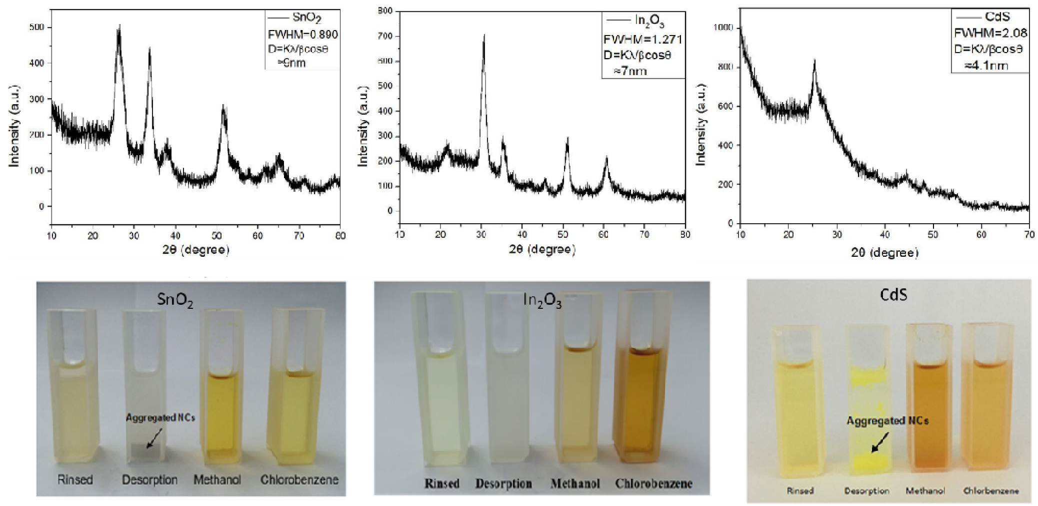

Figure S1. The optical images and XRD patterns of two metal oxides (SnO_2, In_2O_3) and one metal sulfide (CdS) nanoinks prepared by the similar procedures, which can prove the methodological generality.

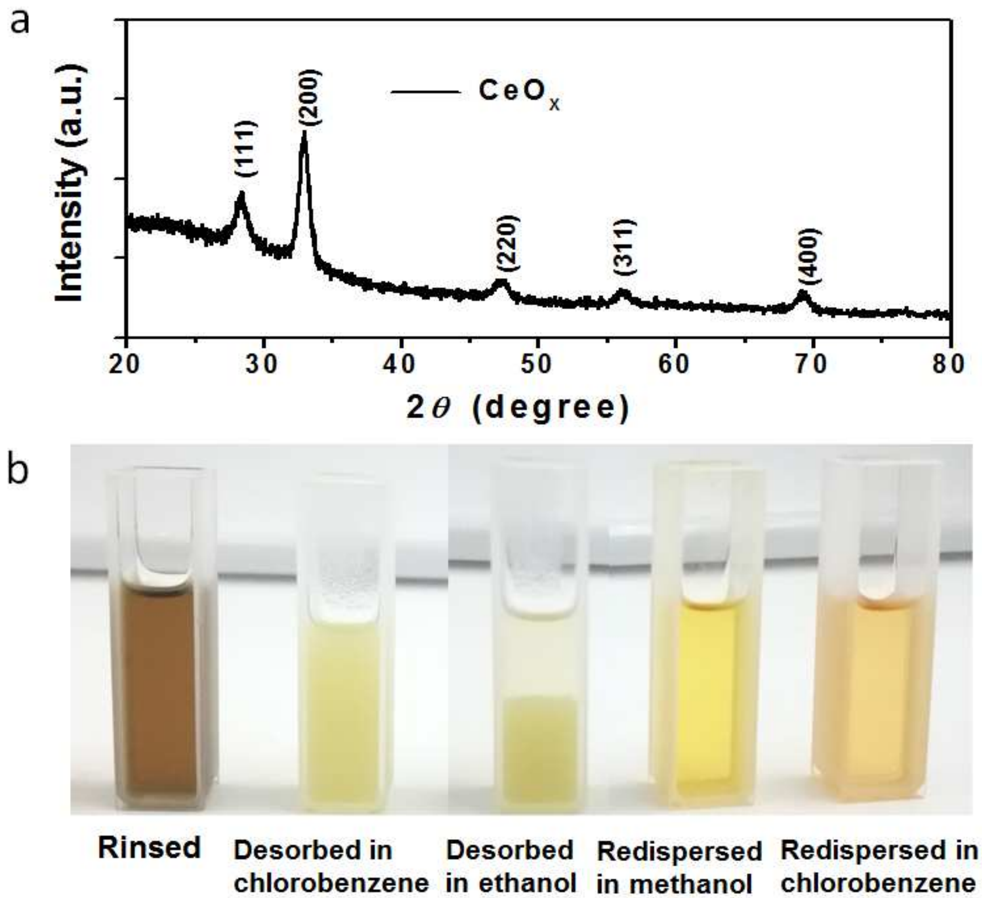

Figure S2. (a) XRD spectrum of the as-synthesized CeO_x nanoparticles. **(b)** Optical images of the rinsed sample in methylbenzene (transparent brown), the desorbed samples in chlorobenzene and ethanol (yellow precipitations), the redispersed samples in methanol (transparent yellow) and chlorobenzene (transparent orange).

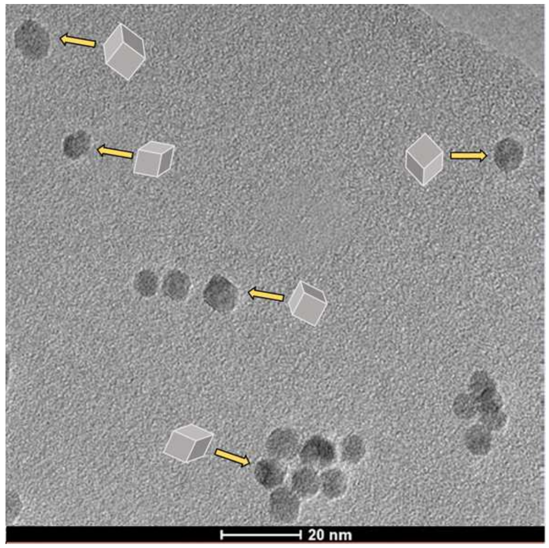

Figure S3. TEM image of CeO_x NCs after surface modification. The cubic shape of the NCs becomes not intuitive due to rotative observation angles, as highlighted by the arrows and the cube insets.

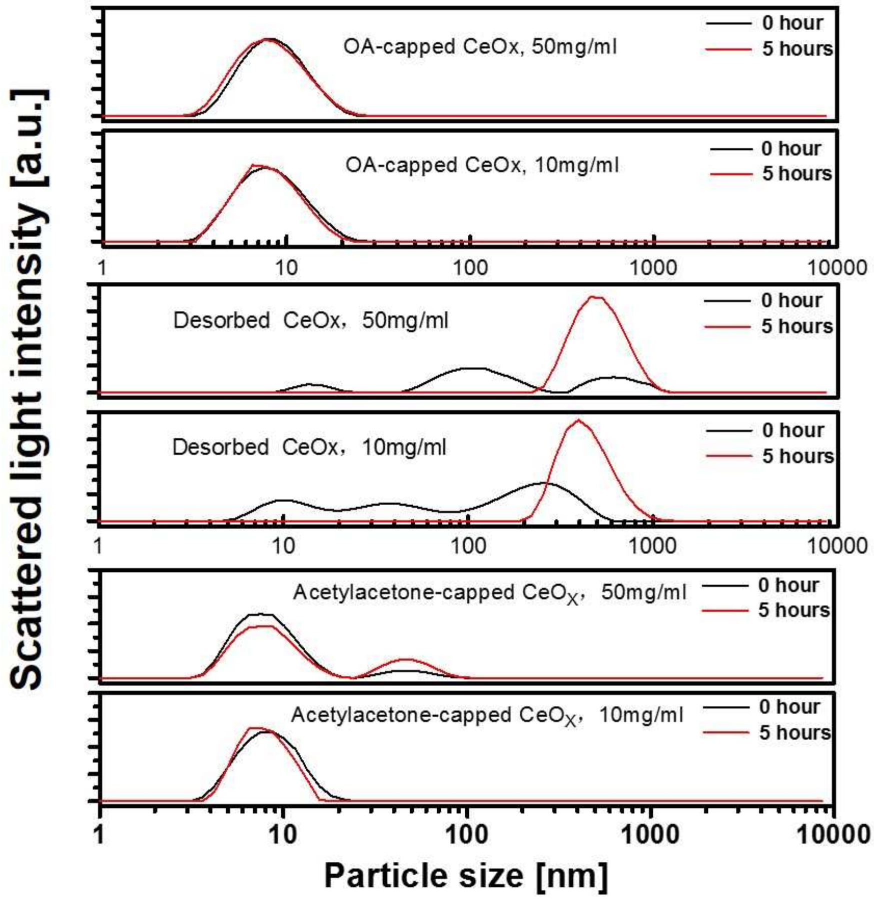

Figure S4. Particle size distributions of nanoinks made of original OA-capped CeO_x NCs, desorbed CeO_x NCs and acetylacetone-capped CeO_x NCs in chlorobenzene with different concentrations. These nanoinks before and after standing for 5 hours are characterized by dynamic light scattering measurement.

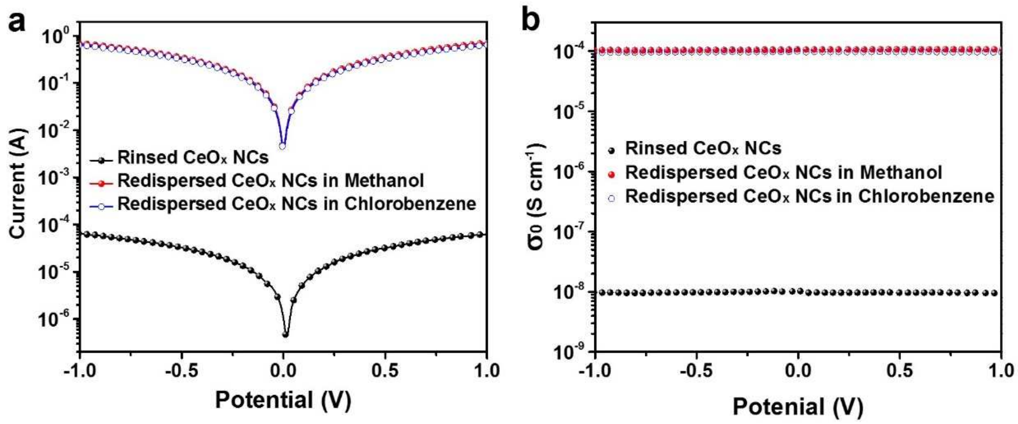

Figure S5. Conductivity measurement of CeO_x nanocrystalline films before and after surface modification. The rinsed sample: OA-capped NCs; the redispersed samples: acetylacetone modified NCs. **(a)** *I-V* curves measured with the device structure of ITO/CeO_x/Ag, with the active area of 0.1 cm^2 and CeO_x film thickness of 150 nm. **(b)** Film conductivity calculated by the equation of $I = \sigma_0 A d^{-1} V$, where I, V, A, d is the measured current, applied potential, sample area and film thickness, respectively.

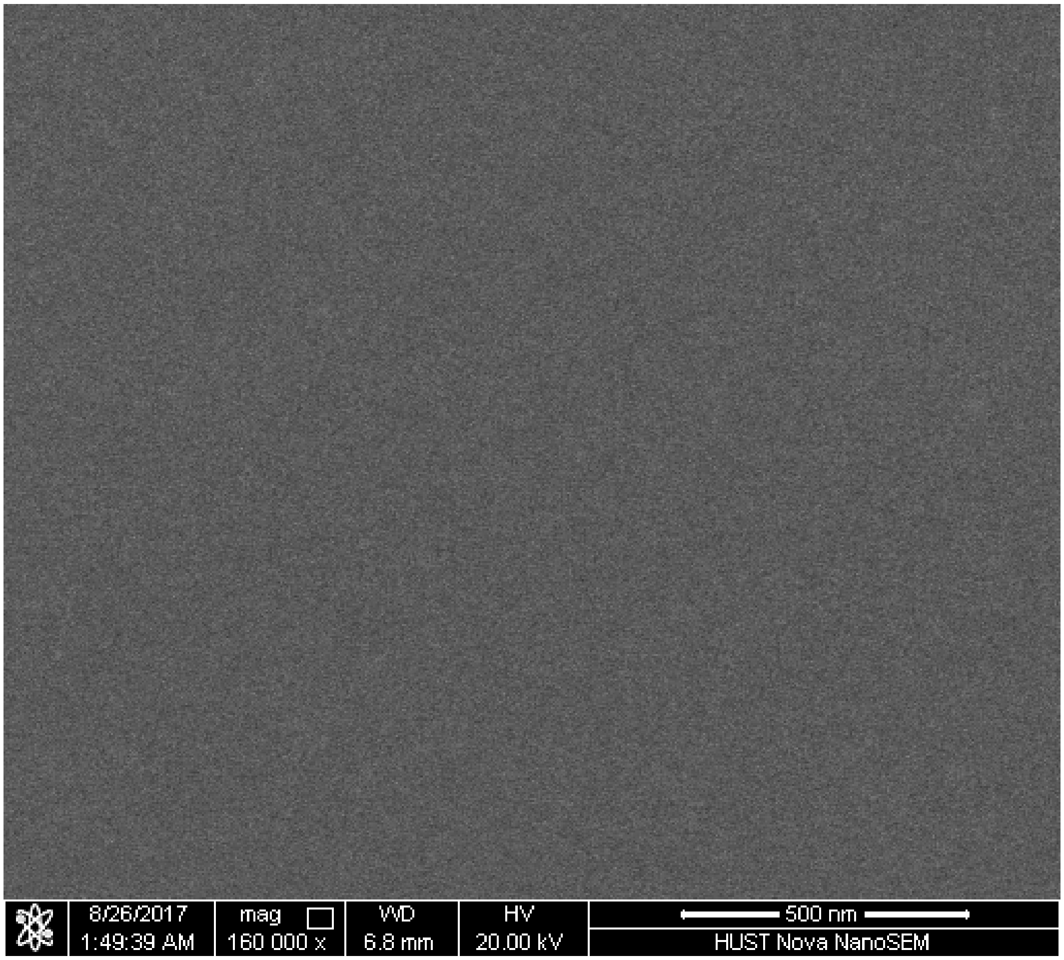

Figure S6. SEM image of the CeO_x nanocrystalline film deposited from its methanol solution on ITO glass substrate. The ultrasmall size of the CeO_x nanocrystals and their closely-packing morphology could be clearly identified.

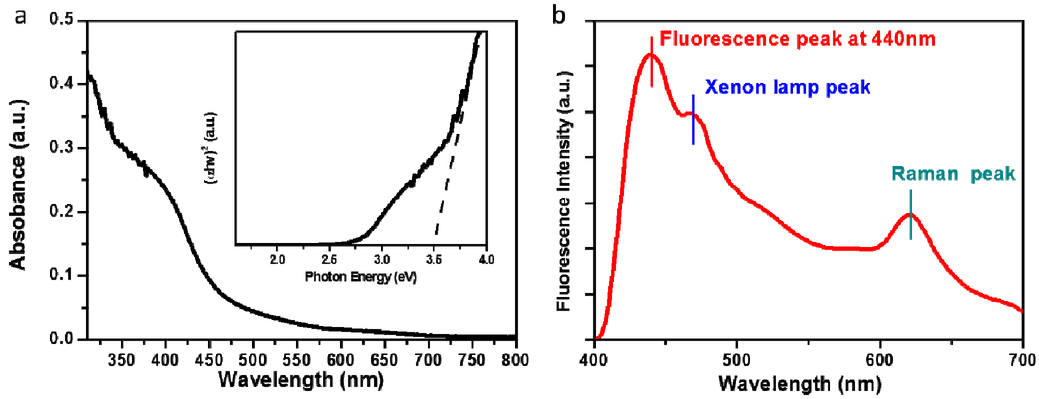

Figure S7. (a) UV-Vis absorption spectrum of the CeO_x film (thickness = 40 nm) and optical band gap of CeO_x determined by the relationship of $(\alpha h\upsilon)^2$ vs photon energy (the inset). **(b)** PL spectrum of the CeO_x nanocrystalline film, excited by 300 nm incident light of a Xenon lamp. The peak at 470 nm is the inherent peak caused by xenon lamp, and the other peak at 620 nm could be assigned to Raman peak excited by incident light.

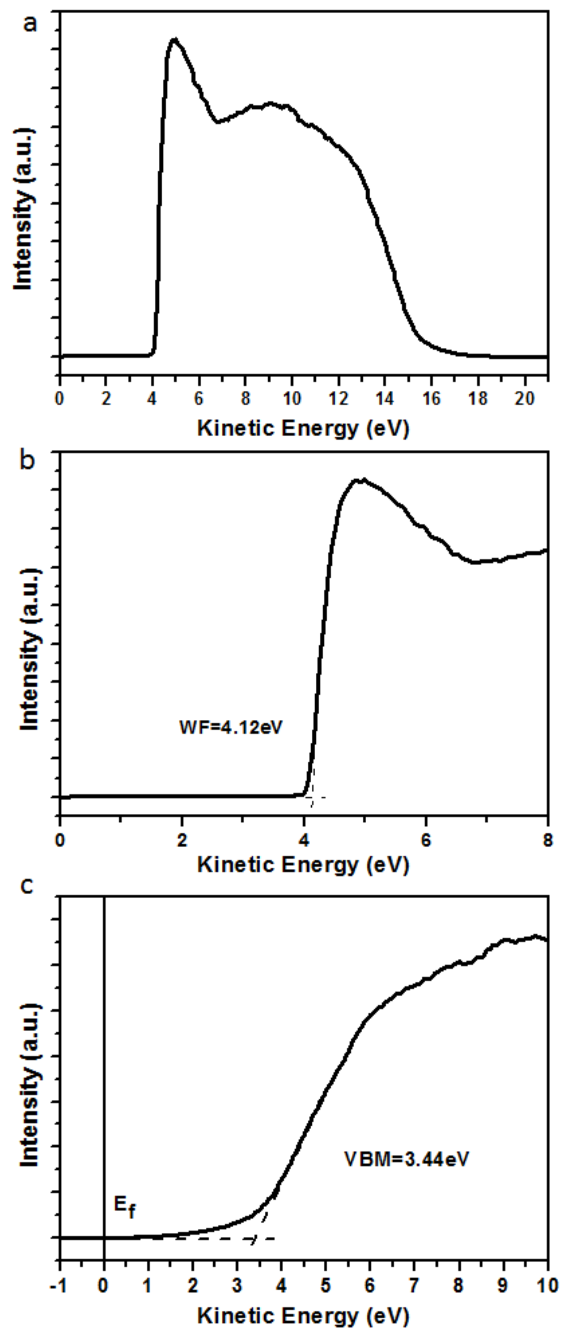

Figure S8. (a) UPS measurement result for the modified CeO_x NCs. **(b)** Work function of CeO_x and **(c)** valence band maximum (VBM) *versus* Fermi level (E_f) of CeO_x measured by UPS.

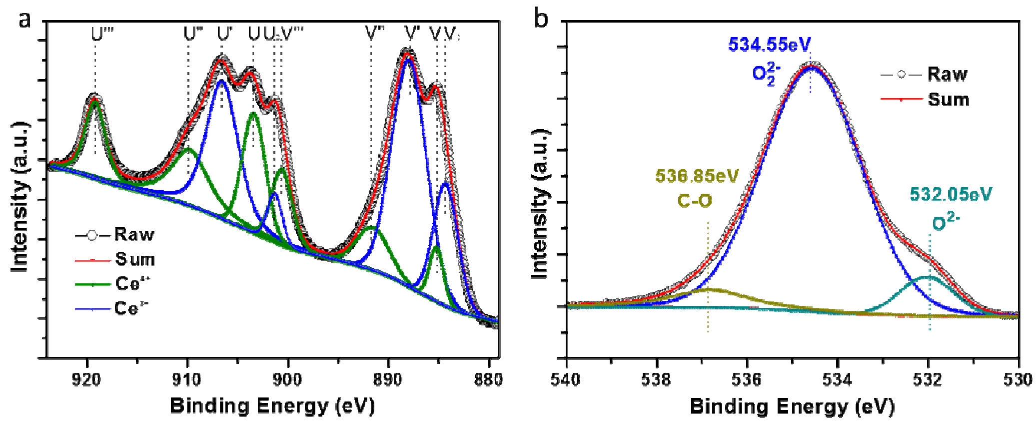

Figure S9. (a) The Ce $3d_{5/2}$ core level XPS spectrum of CeO_x. Three pairs of Spin-orbit doublets of Ce^{4+} are denoted as U'''(V'''), U''(V''), U(V), while two pairs of Spin-orbit doublets of Ce^{3+} are denoted as U'(V') and $U_0(V_0)$. **(b)** The O 1s core level XPS spectrum of CeO_x. O_2^{2-}, O^{2-} are related to lattice O bonded to Ce^{3+} and Ce^{4+} respectively. C-O should come from the surface absorbed acetylacetone.

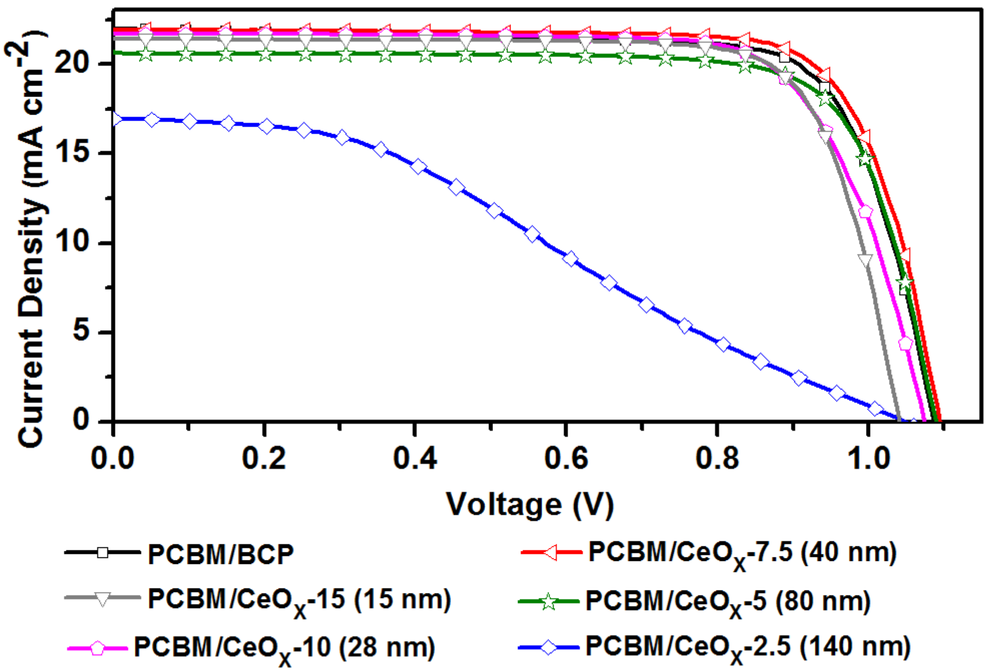

Figure S10. Forward scan *J-V* curves of the devices based on PCBM/BCP and PCBM/CeO_x ETLs with different CeO_x layer thicknesses. The thickness was adjusted by diluting the original methanol solution of surface modified CeO_x NCs with pure methanol. Numbers in the sample labels are the diluted times, corresponding to different thicknesses of CeO_x layers which are denoted in the parentheses.

Table S1. Comparison on the device performance with the structure of FTO/NiMgLiO/$MAPbI_3$/PCBM/CeO_x/Ag, based on thickness controlled CeO_x layers. Numbers in the sample labels are the diluted times of the original CeO_x nanoinks. CeO_x layer thicknesses (as denoted in the parentheses) were measured by a surface profiler by deposition the same nanoinks on glass slides. The performance of the devices based on PCBM and PCBM/BCP reference ETLs have also been given.

Sample	Scanning mode	V_{OC} [V]	J_{SC} [mA cm^{-2}]	*FF*	*PCE* [%]
PCBM	Forward Scan	1.064	21.429	0.656	14.96
	Reverse Scan	1.075	21.296	0.664	15.20
PCBM/BCP (5nm)	Forward Scan	1.085	21.994	0.760	18.13
	Reverse Scan	1.096	21.923	0.760	18.26
PCBM/CeO_x-15 (15 nm)	Forward Scan	1.040	21.429	0.784	17.47
	Reverse Scan	1.083	21.296	0.664	15.32
PCBM/CeO_x-10 (28 nm)	Forward Scan	1.074	21.645	0.793	18.44
	Reverse Scan	1.110	22.061	0.709	17.35
PCBM/CeO_x-7.5 (40 nm)	Forward Scan	1.092	21.897	0.777	18.57
	Reverse Scan	1.115	21.820	0.768	18.69
PCBM/CeO_x-5 (80 nm)	Forward Scan	1.088	20.579	0.767	17.17
	Reverse Scan	1.098	20.441	0.752	16.88
PCBM/CeO_x-2.5 (140 nm)	Forward Scan	1.046	16.995	0.336	5.97
	Reverse Scan	1.048	16.904	0.358	6.34

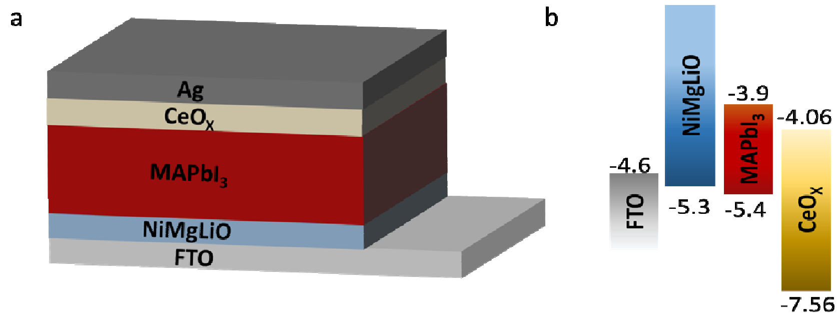

Figure S11. (a) Device structure of the FTO/NiMgLiO/MAPbI$_3$/CeO$_x$/Ag studied in this work, **(b)** energy levels (relative to vacuum) of the various device components.

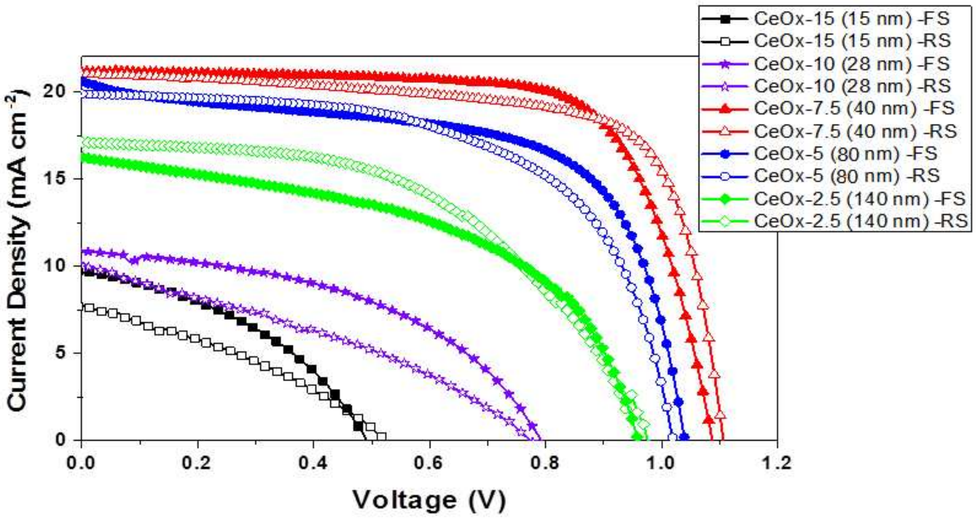

Figure S12. *J-V* curves of the devices based on sole CeO_x ETLs with different CeO_x layer thicknesses, as denoted in the parentheses. FS: forward scan, RS: reverse scan. Too thin or too thick CeO_x layer will not result in optimized performance. Too thin (15-28 nm) CeO_x layer cannot fully cover perovskite underlayer and leads to short-paths between perovskite and Ag electrode. Too thick (140 nm) CeO_x layer with high internal resistance will lead to charge transport problem.

Table S2. Comparison on the device performance based on the structure of FTO/NiMgLiO/$MAPbI_3$/CeO_x/Ag with different CeO_x layer thicknesses as denoted in the parentheses.

Samples	Scanning mode	V_{OC} [V]	J_{SC} [mA cm^{-2}]	*FF*	*PCE* [%]
CeO_x-15 (15 nm)	Forward Scan	0.491	9.61	0.409	1.93
	Reverse Scan	0.525	7.72	0.335	1.36
CeO_x-10 (28 nm)	Forward Scan	0.791	10.86	0.466	4.01
	Reverse Scan	0.778	10.20	0.329	2.61
CeO_x-7.5 (40 nm)	Forward Scan	1.085	21.13	0.721	16.54
	Reverse Scan	1.112	20.99	0.714	16.65
CeO_x-5 (80 nm)	Forward Scan	1.032	20.47	0.635	13.39
	Reverse Scan	1.012	19.86	0.606	12.17
CeO_x-2.5 (140 nm)	Forward Scan	0.961	16.23	0.503	7.85
	Reverse Scan	0.975	17.10	0.513	8.48

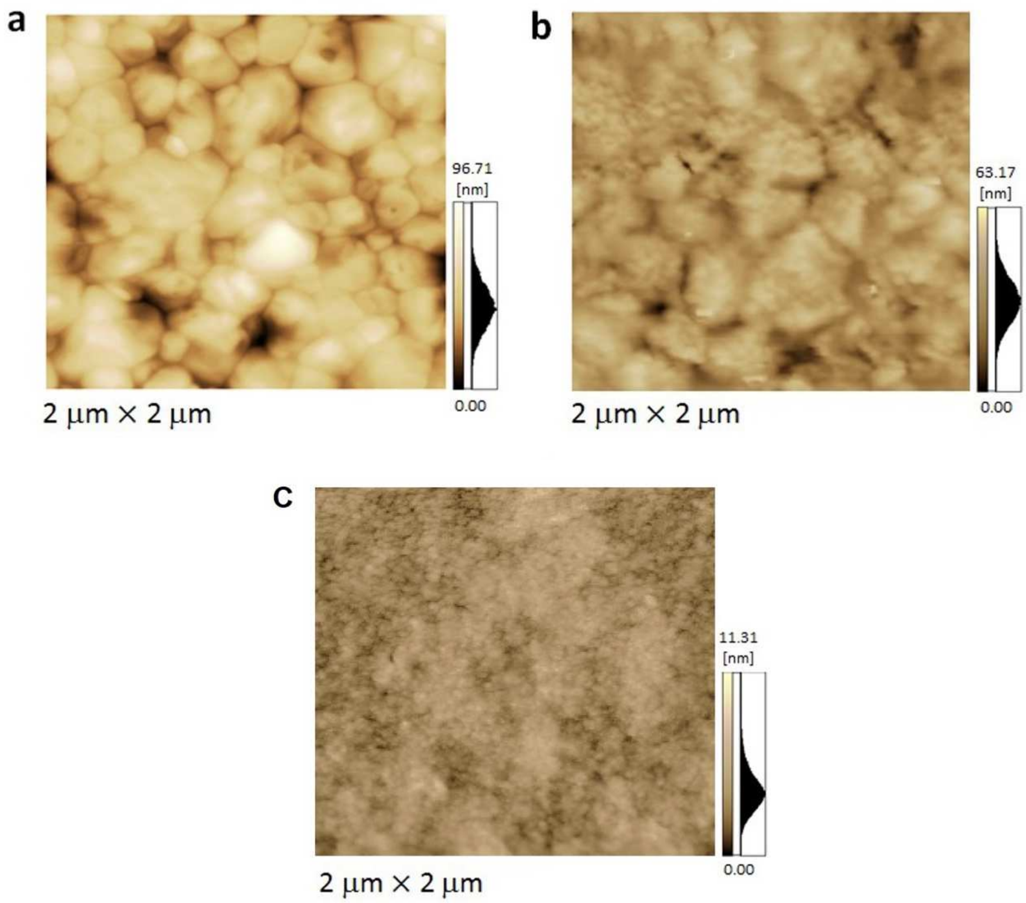

Figure S13. AFM images of **(a)** a bare perovskite film, **(b)** a 15 nm-thick CeO_x layer on perovskite film, **(c)** a 40 nm-thick CeO_x layer on perovskite film. The surface roughnesses for the films in (a-c) are 32.18 nm, 21.63 nm, and 2.16 nm, respectively. Obviously, the 15 nm-thick CeO_x layer is too thin to fully cover the perovskite layer's rough surface; the 40 nm-thick CeO_x layer is thick enough to fully cover the perovskite underlayer.

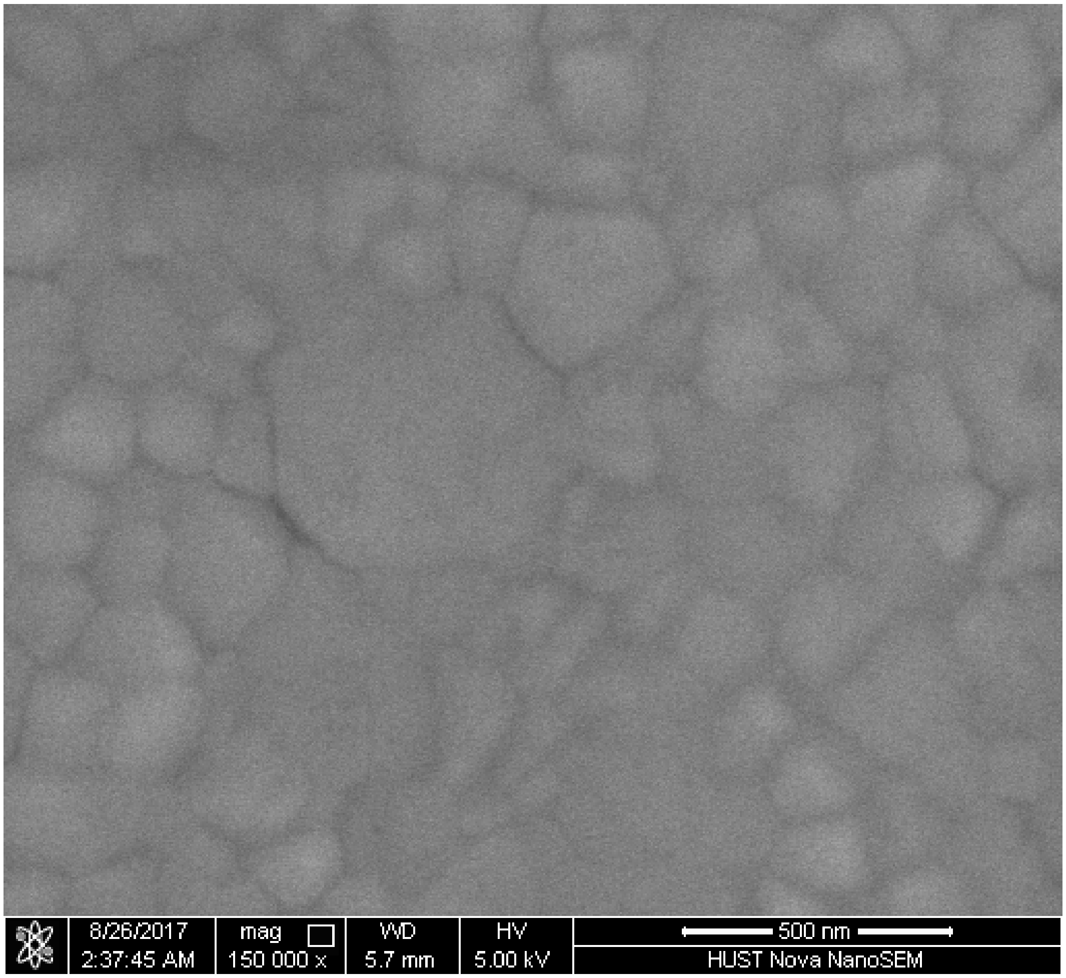

Figure S14. SEM image of perovskite film homogeneously covered by a pin-hole free 40 nm-thick CeO_x layer made of acetylacetone modified CeO_x NCs.

Table S3. Comparison on the device performance based on the structure of FTO/NiMgLiO/$MAPbI_3$/CeO_x/Ag and CeO_x NCs before (rinsed sample) and after (modified sample) acetylacetone surface modification. The CeO_x layer thicknesses were controlled the same at 40 nm.

Samples	Scanning mode	V_{OC} [V]	J_{SC} [mA cm^{-2}]	*FF*	*PCE* [%]
Rinsed CeO_x	Forward Scan	0.987	12.221	0.262	3.15
	Reverse Scan	0.987	11.598	0.319	3.66
Modified CeO_x	Forward Scan	1.085	21.134	0.721	16.54
	Reverse Scan	1.112	20.993	0.714	16.65

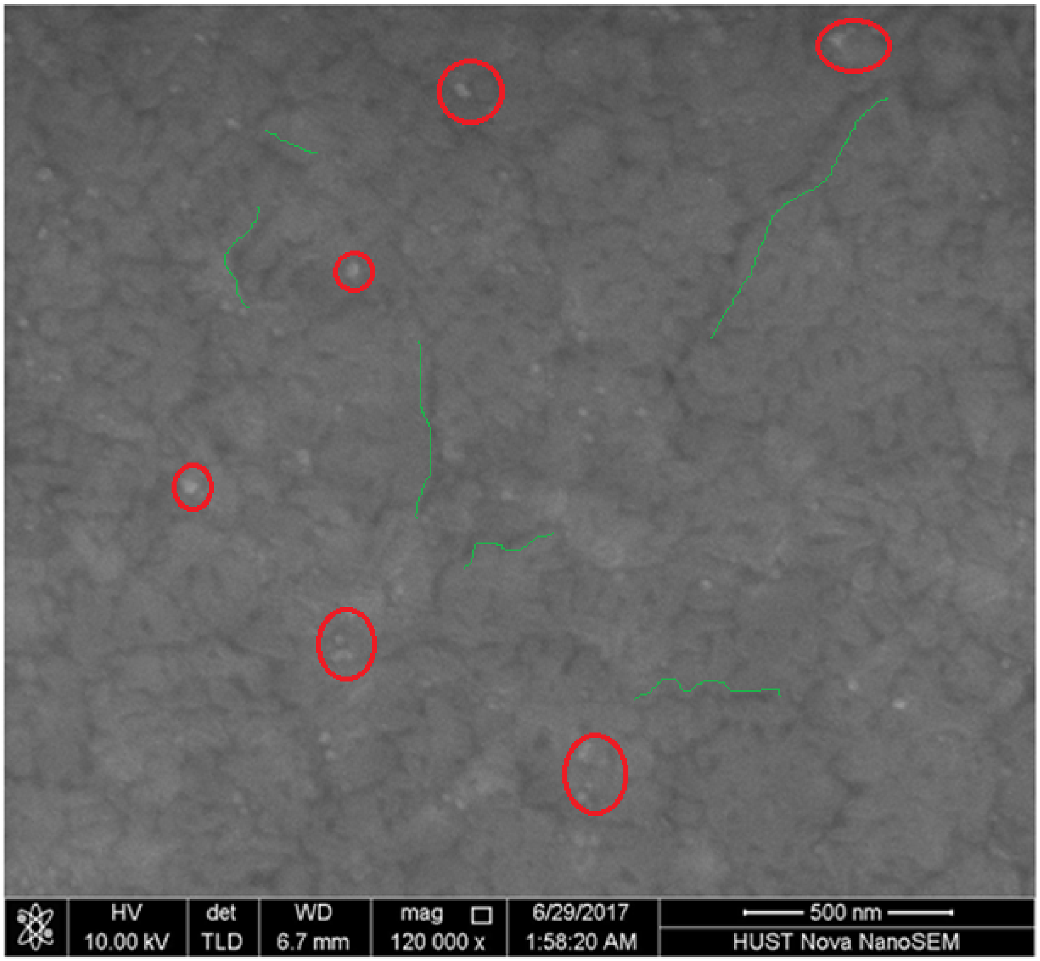

Figure S15. SEM image of perovskite film covered by a 80 nm-thick CeO_x layer made of desorbed CeO_x NCs without any surface-capping agents. Aggregates in the film have been highlighted by the red circles, worm-like cracks have been denoted by the green lines. This film morphology may be associated with poor dispersity of the spin-coating precursor, *i.e.*, the desorbed CeO_x NCs in chlorobenzene (10 mg ml^{-1}).

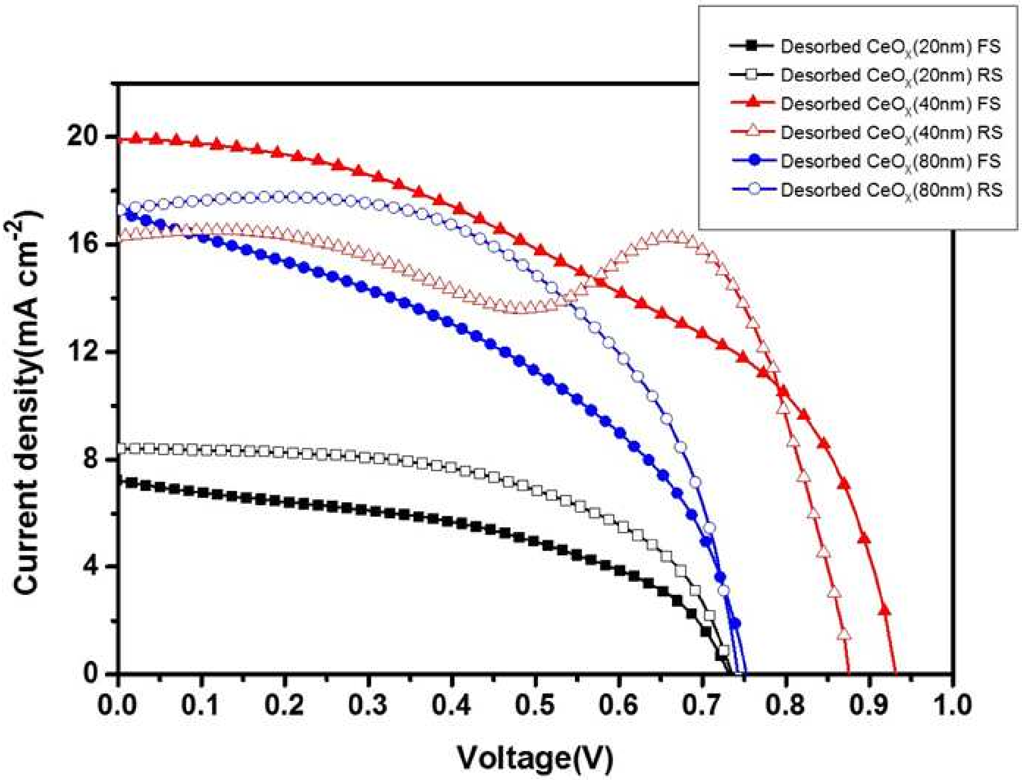

Figure S16. *J-V* curves of the devices based on the desorbed CeO_x ETLs with different thicknesses, as denoted in the parentheses. FS: forward scan, RS: reverse scan. The desorbed CeO_x ETL was deposited on top of perovskite by spin-coating chlorobenzene solution of the desorbed CeO_x NCs (10 mg ml^{-1}) without any surface-capping agents. After ultrasonic treatment and then resting for several minutes, the upper part of clear solution was used for spin-coating. Different film thickness was achieved by repeating this spin-coating procedure.

Table S4. Comparison on the devices performance with the structure of FTO/NiMgLiO/$MAPbI_3$/d-CeO_x/Ag based on the desorbed CeO_x (d-CeO_x) ETLs with different thicknesses.

Samples	Scanning mode	V_{OC} [V]	J_{SC} [mA cm^{-2}]	*FF*	*PCE* [%]
d- CeO_x (20 nm)	Forward Scan	0.732	7.23	0.466	2.47
	Reverse Scan	0.734	8.39	0.562	3.46
d- CeO_x (40 nm)	Forward Scan	0.930	19.93	0.479	8.88
	Reverse Scan	0.875	16.25	0.778	11.06
d- CeO_x (80 nm)	Forward Scan	0.778	17.49	0.437	5.95
	Reverse Scan	0.799	16.93	0.612	8.28

Table S5. Summary on all-inorganic interfacial layer based PVSCs with different structures in the reports.

PCE	Cell configuration	Structure	Reference
20.4%	$FTO/TiO_2/MAPbI_3/CuSCN/Au$	meso/regular	Science, 2017, DOI:10.1126/science.aam5655
16.6%	$FTO/TiO_2/MAPbI_3/CuSCN/Au$	meso/normal	ACS Energy Lett. 2016, 1, 1112.
13%	$ITO/NiO/MAPbI_3/Bi_2S_3/Au$	planar/inverted	ACS Photonics. 2016, 3, 2122.
6.0%	$FTO/TiO_2/MAPbI_3/CuI/Au$	meso/regular	J. Am. Chem. Soc., 2014, 136, 758.
15.9%	$FTO/TiO_2/Al_2O_3/Carbon$ ($MAPbI_3$-$SrCl_2$)	meso/regular	Adv. Mater., 2017, 29, 1606608 (our previous work)
18.5%	$FTO/TiO_2/MAPbI_3/CuGaO_2/Au$	planar/regular	Adv. Mater., 2017, 29, 1604984 (our previous work)
16.1%	$FTO/NiO/MAPbI_3/ZnO/Ag$	planar/inverted	Nat. Nanotechnol., 2016, 11, 75.
16.7%	$FTO/NiMgLiO/MAPbI_3/CeO_x/Ag$	planar/inverted	**This work**

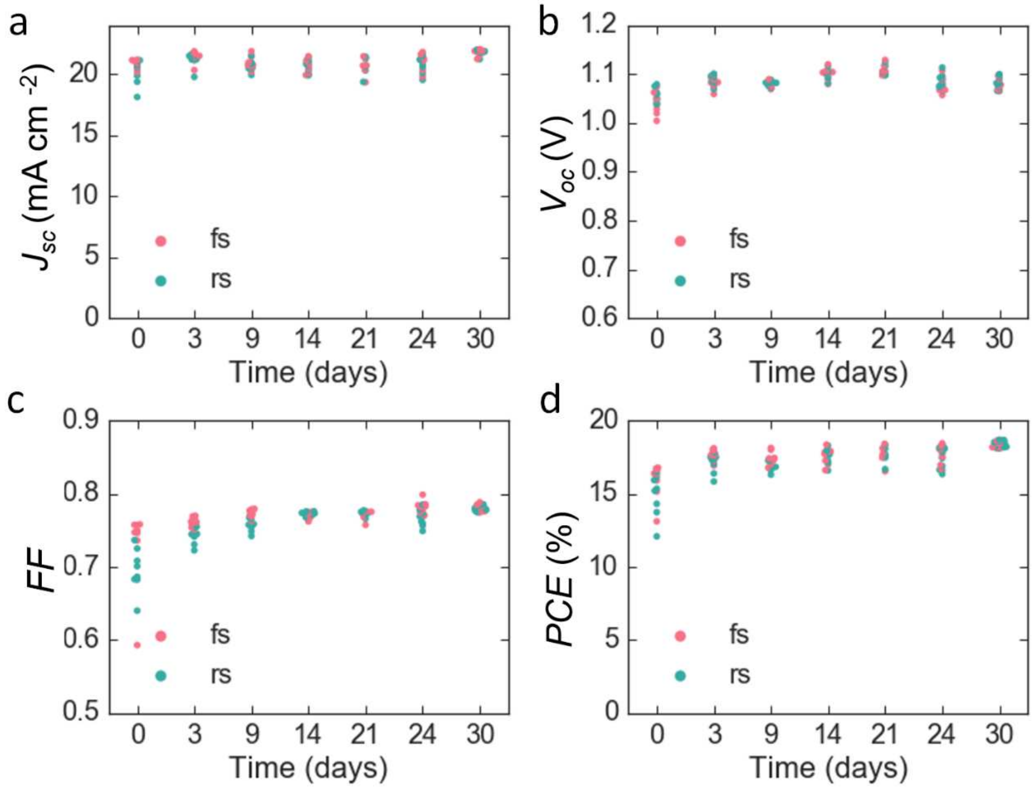

Figure S17. Performance evolution of the unencapsulated devices with the structure of FTO/NiMgLiO/$MAPbI_3$/PCBM/CeO_x (40 nm)/Ag during 30 days, which were stored in the dark and air with controlled humidity of 30% and tested in ambient air without humidity control.

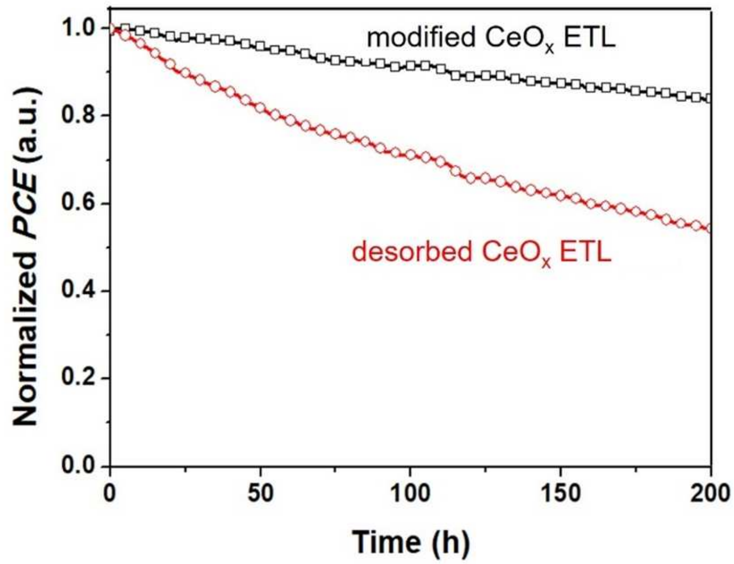

Figure S18. Normalized *PCE*s of the PVSCs based on the acetylacetone modified CeO_x ETL (40 nm) and the desorbed CeO_x ETL (40 nm). The unencapsulated devices were aging for 200 hours in a N_2 filled glovebox under continuous light soaking and maximum power point tracking.

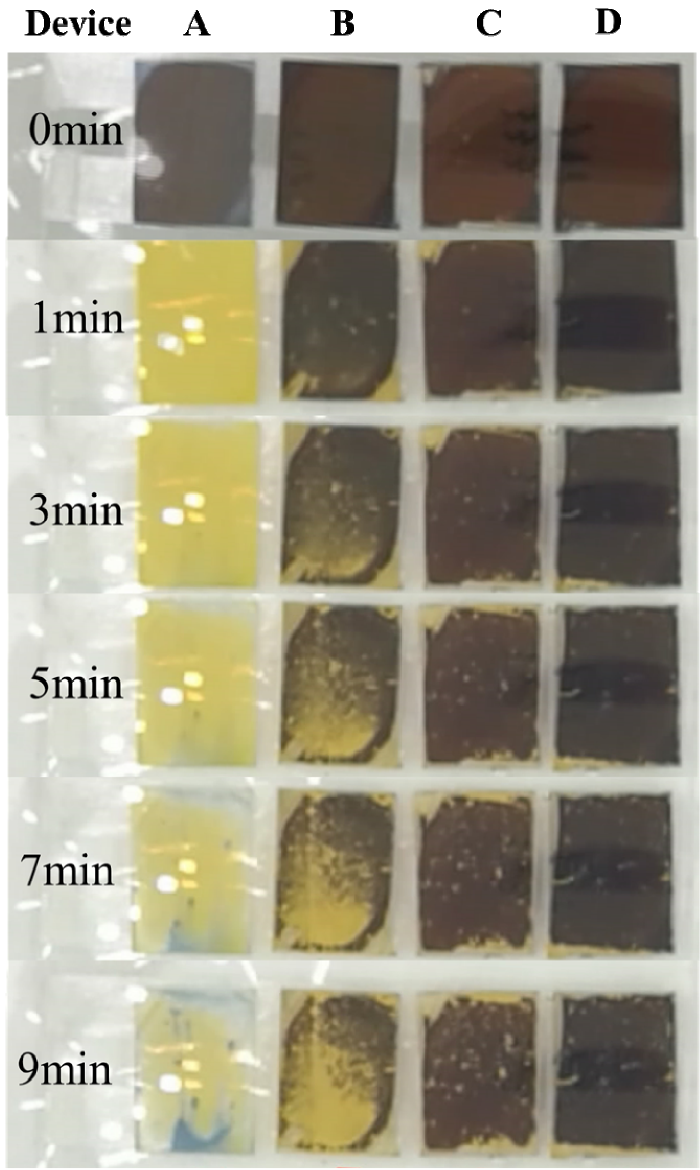

Figure S19. Comparison on the waterproof capability of different ETLs by immersing the films directly in water for ~10 minutes. Perovskite films without and with different ETLs covering on top have been compared. Sample A: bare $MAPbI_3$ film, Sample B: $MAPbI_3$/PCBM, Sample C: $MAPbI_3$/PCBM/BCP (5 nm), Sample D: $MAPbI_3$/PCBM/CeO_x (40 nm). The color changed from dark brown to light yellow, reflecting the decomposition of $MAPbI_3$ to PbI_2. The whole process has been recorded in **Video S1**.

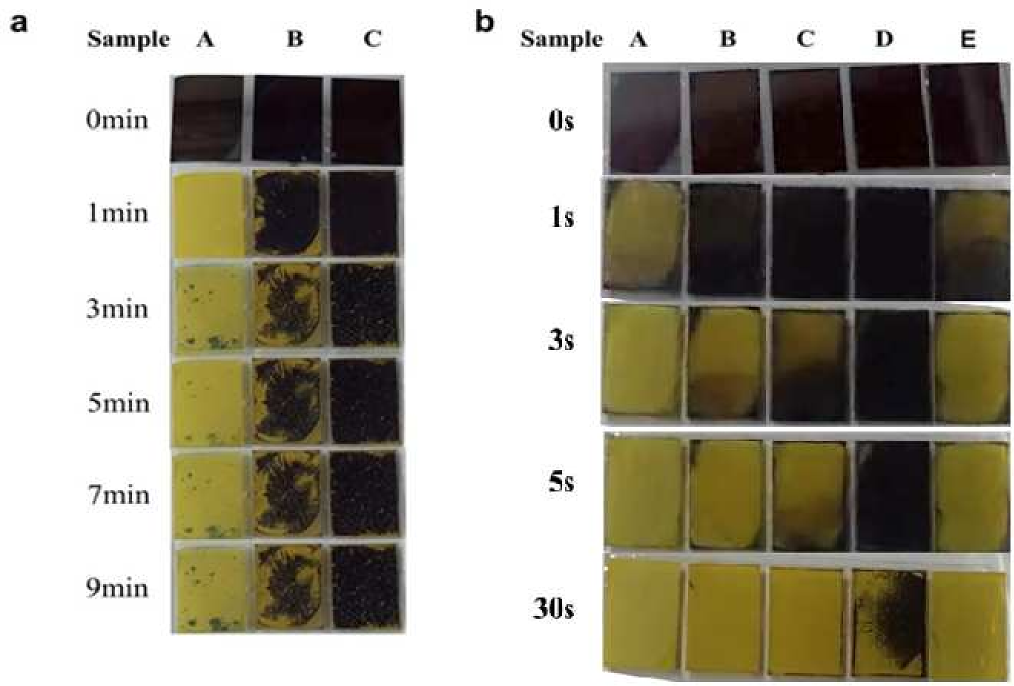

Figure S20. Comparison on the waterproof capability of two group ETLs with their thicknesses controlled the same by immersing them directly in water for several minutes. Perovskite films without and with different ETLs covering on top have been compared. (a) Group I: Sample A: bare $MAPbI_3$ film, Sample B: $MAPbI_3$/PCBM (100 nm), Sample C: $MAPbI_3$/PCBM (60 nm)/BCP (40 nm), the whole process has been recorded in **Video S2**. (b) Group II: Sample A: bare $MAPbI_3$ film, Sample B: $MAPbI_3$/BCP (40 nm), Sample C: $MAPbI_3$/modified CeO_x (40 nm), Sample D: $MAPbI_3$/PCBM (40 nm), Sample E: $MAPbI_3$/desorbed CeO_x (40 nm), the whole process has been recorded in **Video S3**.

By comparing **Figure S**19, **S**20, it is known that the order of water-proof capability for the different ETLs should be PCBM (60nm)/CeO_x (40nm) ≈ PCBM (60nm)/BCP (40nm) > PCBM (60nm)/BCP (5nm) >> PCBM (100 nm) > PCBM (40 nm) >> modified CeO_x (40 nm) > BCP (40nm) > desorbed CeO_x (40 nm). It is interesting that sole CeO_x and sole BCP are less hydrophobic and not better than sole PCBM for water-proof, but the bilayer structures of both PCBM(60 nm)/BCP (40 nm) and PCBM(60 nm)/CeO_x (40 nm) are much superior in water-proof than sole PCBM (100 nm), even though their total thicknesses have been controlled the same at 100 nm. These indicate the structural advantage of bilayer ETLs for water-proof cannot be simply realized by increasing single layer's thickness of PCBM. It is thought that the PCBM layer's pinholes might be blocked by the upper layer of BCP or CeO_x, while such kind pinholes could not be removed in single layer of PCBM even though its thickness is much increased.

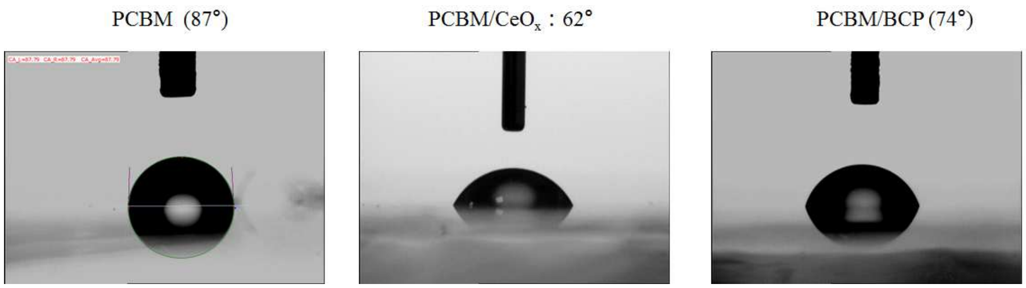

Figure S21. The water contact angles of PCBM, PCBM/CeO_x (modified by acetylacetone) and PCBM/BCP.

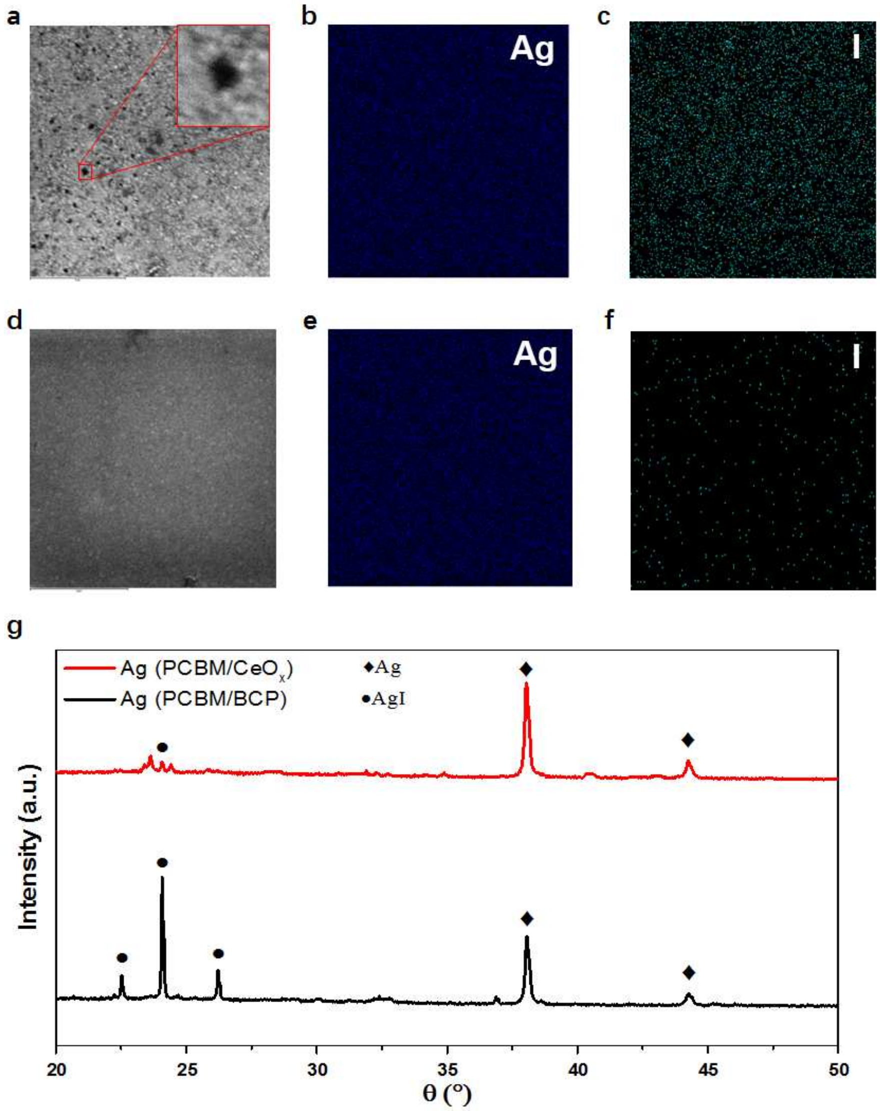

Figure S22. SEM images and EDX mapping results of the Ag electrodes peeled off from the aged samples of **(a-c)** "FTO/NiMgLiO/MAPbI$_3$/PCBM/BCP (5 nm) /Ag" and **(d-f)** "FTO/NiMgLiO/MAPbI$_3$/PCBM/CeO$_x$ (40 nm)/Ag". Their XRD patterns are shown in (**g**). The samples were firstly aged at 100 °C for 24 hours. And then, the Ag electrodes were peeled off by immersing the samples in chlorobenzene. The inner surface of Ag electrode in the PCBM/BCP based sample has a lot of pin-holes and is seriously contaminated by iodine due to the corrosion reaction between perovskite species and Ag. This leads to the formation of AgI. In the contrast, the corrosion of the inner surface of Ag electrode in the PCBM/CeO_x based sample is much slighter. The results prove that the PCBM/CeO_x (40 nm) bilayer has better chemical shielding effect than the PCBM/BCP (5 nm) bilayer, which can effectively block the diffusion paths between $MAPbI_3$ layer and Ag electrode.

Additional files: Video S1-S3. These videos recorded the color change of perovskite films without and with different ETLs covering on top by immersing them directly in water for several minutes.